

Effects of biaxial strain on the impurity-induced magnetism in P-doped graphene and N-doped silicene: A first principles study

J. Hernández-Tecorralco¹, L. Meza-Montes¹, M. E. Cifuentes-Quintal², and R. de Coss²

¹ Instituto de Física, Benemérita Universidad Autónoma de Puebla, Apartado Postal J-48, 72570, Puebla, Puebla, México

² Departamento de Física Aplicada, Centro de Investigación y de Estudios Avanzados del IPN, Apartado Postal 73, Cordemex, 97310, Mérida, Yucatán, México

E-mail: romeo.decoss@cinvestav.mx

Abstract.

The effects of biaxial strain on the impurity-induced magnetism in P-doped graphene (P-graphene) and N-doped silicene (N-silicene) are studied by means of spin-polarized density functional calculations, using the supercell approach. The calculations were performed for three different supercell sizes 4×4 , 5×5 , and 6×6 , in order to simulate three different dopant concentrations 3.1, 2.0 and 1.4%, respectively. For both systems, the calculated magnetic moment is $1.0 \mu_B$ per impurity atom for the three studied concentrations. From the analysis of the electronic structure and the total energy as a function of the magnetization, we show that a Stoner-type model describing the electronic instability of the narrow impurity band accounts for the origin of *sp*-magnetism in P-graphene and N-silicene. Under biaxial strain the impurity band dispersion increases and the magnetic moment gradually decreases, with the consequent collapse of the magnetization at moderate strain values. Thus, we found that biaxial strain induces a magnetic quantum phase transition in P-graphene and N-silicene.

Keywords: *sp magnetism, magnetic phase transition, graphene, silicene, strain, doping*

1. INTRODUCTION

Magnetism is one of the most studied phenomena in physics and materials science. The magnetic behavior of the matter is usually attributed to the presence of *d*- or *f*-electrons. However, less common is the existence of magnetic materials with only *s*- and *p*-electrons. The arise of graphene [1] and related two-dimensional (2D) materials, such as silicene, have aroused great interest due to their outstanding properties and the expectation to exhibit *sp*-magnetism under certain conditions. Pristine graphene and silicene are non-magnetic, however, an alternative to induce magnetism is by introducing defects. For instance, it has been observed that vacancies [2] or the chemical functionalization using adsorbed [2, 3, 4] or substitutional [5] impurities, are effective ways to induce magnetism in 2D systems. Thus, the study of impurity-induced magnetism in low-dimensional materials is relevant in view of their potential applications in spintronics [6, 7] and spin-based quantum information systems [8, 9].

The electronic and magnetic properties of doped graphene and silicene with substitutional *sp*-impurities; Al, Si, P, and S, for graphene and B, N, Al, and P for silicene, have been theoretically studied using first principles calculations based on the density functional theory [10, 11, 12, 13, 14]. Particularly, it has been reported that phosphorus and nitrogen atoms as single substitutional impurities in graphene (P-graphene) and silicene (N-silicene), respectively, present a net magnetic moment. Dai *et al.* [10, 11] report a net magnetic moment of $1.05 \mu_B$ in P-graphene for doping concentrations of 1.4 and 3.1 %. The P atom introduces a local curvature in the graphene lattice and they report a metastable non-magnetic state when the P atom is at the plane. Wang *et al.* [12] obtain similar results at a doping concentration of 2 % with magnetic moment of $1.02 \mu_B$. The authors attribute the origin of the magnetism to the symmetry breaking of π -electrons in graphene. Furthermore, they show that the spin density charge is distributed over the whole lattice. A systematic study of the concentration effect in graphene with *sp*-impurities as Al, Si, P, and S was performed by Denis [13]. These results show that for P-graphene the magnetic moment is independent of the concentration in a range of 0.8-3.1 %. It is important to mention that within the group of impurities Al, Si, P and S, only the P impurity induces magnetism in graphene.

For doped silicene, the effects of the chemical functionalization with B, N, Al and P impurities for a doping concentration of 3.1 % were analyzed by Sivek *et al.* [14], using the density functional theory with the local density approximation for the exchange-correlation potential. Their results showed that the nitrogen substitutional impurity induces a magnetic moment of $0.9 \mu_B$ and the system is vibrationally stable. The authors also discuss that the contribution of *s*- and *p*-states of N gives rise to metallic bands in silicene. Hence, in a similar way that for P-graphene, Sivek *et al.* [14] found that within the group of impurities B, N, Al, and P, only the N impurity induces magnetism in silicene. Thus, first-principles calculations predict that P-graphene and N-silicene belong to the group of *sp*-magnetic systems. However, the details of the mechanism that gives rise the magnetism in P-graphene and N-silicene still needs to be

fully understood.

Additionally, having a technique that allows us to modulate the magnetic properties of 2D materials is highly desirable. In this way, it has been showed that strain engineering is an effective method to modulate the electronic and magnetic properties in transition metal doped 2D systems [15, 16, 17]. Nevertheless, the study of strain effects on the impurity-induced *sp*-magnetism in P-graphene or N-silicene is still lacking. Thus, a systematic and comparative theoretical study of the magnetic properties in P-graphene and N-silicene is necessary in order to understand the effect of strain for different dopant concentration values.

Therefore, the aim of this work is to contribute to the understanding of the impurity-induced magnetism in P-graphene and N-silicene and how the magnetic moment of these systems could be modulated under a positive isotropic deformation (biaxial strain). Here, we present results of first-principles calculations based on the Density Functional Theory (DFT) for the structural, electronic and magnetic properties of P-graphene and N-silicene for three different doping concentrations (3.1, 2.0 and 1.4%) in a moderate range of deformations (0 – 10%). Firstly, the first-principles results for the electronic structure and the total-energy as a function of the magnetization are analyzed using a Stoner-type model describing the electronic instability of a narrow impurity band, and we show that this model accounts for the origin of *sp*-magnetism in P-graphene and N-silicene. Secondly, the results for the evolution of the magnetic moment as a function of the biaxial strain are presented. We find that biaxial strain gradually destabilizes the magnetic state inducing a magnetic to paramagnetic phase transition in these systems. The paper is structured as follows: In Sec. II we describe the computational details of our calculations. In Sec. IIIA structural results are presented and the magnetic and electronic properties are discussed in Sec. IIIB. Finally, in Sec. IV we report our main conclusions. Particularly useful is Appendix A presenting a detailed description of the narrow impurity band model for ferromagnetism used throughout the paper.

2. Computational details

The DFT calculations were performed within the framework of the plane-waves pseudopotential approach, as implemented in the QUANTUM-ESPRESSO code [18]. Core electrons were replaced by ultrasoft pseudopotentials taken from the **PSlibrary** 1.0.0 database [19] and the valence wave functions (charge density) were expanded in plane waves with a kinetic-energy cutoff of 55 (340) Ry for graphene and 50 (320) Ry for silicene. The exchange-correlation functional was treated with the Perdew-Burke-Enzerhof [20] parametrization of the generalized gradient approximation. Since our study systems involve only *s* and *p* electrons, we expect that this functional provides a good description of the magnetic behavior, compared with cases with highly localized *d* or *f* orbitals, where usually tends to give a poor description due to an effect of delocalization of the wavefunctions. We simulated P (N) substitutional impurities by replacing one C (Si) atom from the graphene (silicene) pristine lattice. We considered

4×4 , 5×5 and 6×6 supercells, with 32, 50, and 72 atoms which correspond to 3.1, 2.0 and 1.4 % of impurities concentrations (c), respectively. For each concentration we calculate the corresponding ground-state lattice constant a_0 by a direct minimization of the electronic total energy. Biaxial tensile strain ε was applied by increasing the lattice constant as $a = (1 + \varepsilon)a_0$. During all the structural calculations the atomic positions were relaxed until the internal forces were less than 0.01 eV/Å. In order to simulate an isolated layer, we left at least 15 Å of vacuum space between periodic images. Special attention was paid to the sampling of the Brillouin zone. For structural calculations, we used a 9×9 k-grid [21] with a Methfessel-Paxton smearing of 0.015 Ry [22]. However, for electronic and magnetic properties we had to use a 18×18 k-grid with a smearing of 0.005 and 0.002 Ry for graphene and silicene, respectively. This was needed in order to properly converge the magnetic moment up to 0.01 μ_B .

3. Results and discussion

3.1. Energetics and structural properties

We begin our discussion by analyzing the energetic stability of the impurity on the host. For that, the binding energy for the unstrained ground state was calculated as

$$E_B = E_{system} - (E_{2D-vacancy} + E_{atom}) , \quad (1)$$

where E_{system} is the total energy of the full relaxed doped system, whereas $E_{2D-vacancy}$ is the total energy for a full relaxed vacancy and E_{atom} is the total energy for the isolated impurity-atom, in this case P or N. For P-graphene we found for E_B values of -8.30 eV, -8.34 eV and -8.42 eV, for the concentrations of 1.4, 2.0, and 3.1 %, respectively, which are in good agreement with the value of -8.31 eV reported by Pašti *et al.* [23]. In the case of N-silicene E_B is -7.24 eV, -7.25 eV and -7.22 eV, for the concentrations of 1.4, 2.0, and 3.1%, respectively. Thus, the calculated values for the binding energy show that the substitutional impurity of P(N) is energetically stable in graphene (silicene).

With respect to the structural properties, it is important to remember that pristine graphene is a flat crystal whereas pristine silicene has a buckled structure. Thus, because of the different structural character and the contrasting size of the impurity atom in each case, a different structural behavior for P-graphene and N-silicene is anticipated. The lattice structure for P-graphene in the ground (unstrained) state shows significant distortions owing to the presence of substitutional P, which has an atomic size larger than the carbon atom. The impurity causes a distorted tetrahedral-type structure with a bond angle of $\theta_{CPC} = 100^\circ$ and P-C bond length of 1.76 Å which is larger than the C-C bond in pristine graphene (1.42 Å). For N-silicene, because N atom is smaller in size than Si, as substitutional impurity it has a N-Si bond length smaller than Si-Si, given by 1.83 Å and 2.27 Å, respectively. The difference in distances causes a bond angle $\theta_{SiNSi} = 119.4^\circ$, which is close to the typical value of sp^2 hybridization whereas for pristine silicene the $\theta_{SiSiSi} = 116.2^\circ$ is usually attributed to sp^2 - sp^3 hybridization. The main structural difference is localized around the impurity, for P-graphene the P

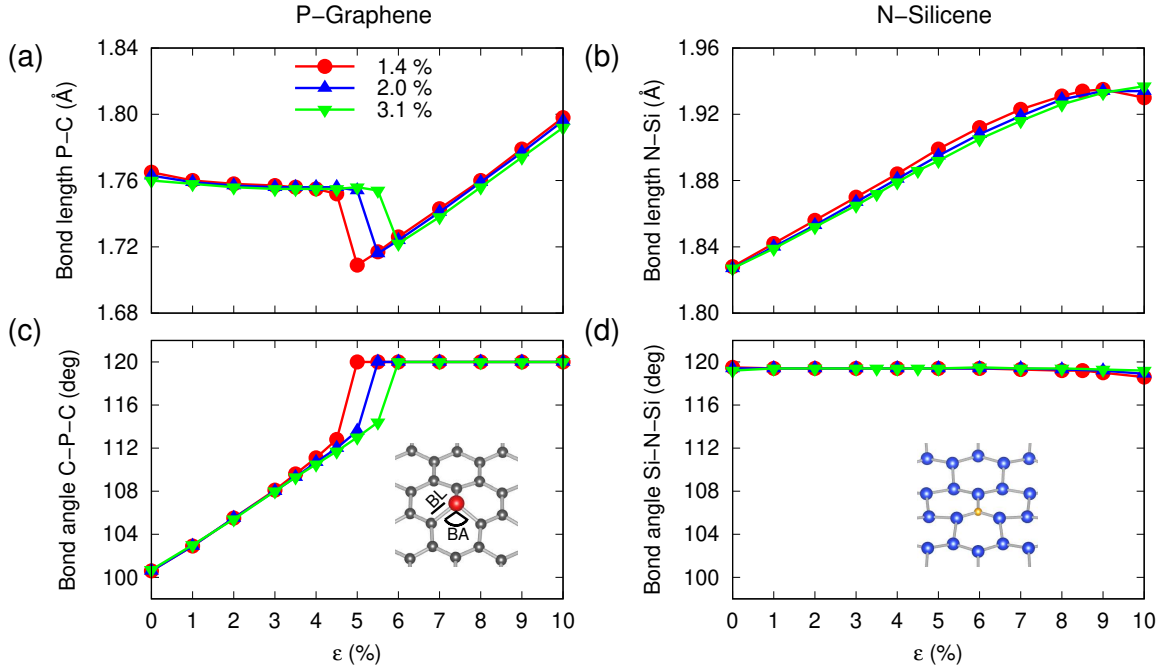


Figure 1. Bond length and bond angle for P-graphene(a, c) and N-silicene (b, d) as a function of deformation ϵ , at the three studied concentrations (1.4, 2.0, and 3.1%).

atom is out of the plane respect to the flat graphitic lattice whereas for N-silicene the N atom is in the same plane with their three first nearest neighbors of a deformed buckled structure. That is the reason for the different evolution of the structural parameters as a function of the biaxial strain for each system as it can be seen in Fig. 1.

For both systems, the evolution of the bond length (BL) and the bond angle (BA) is almost independent of the concentration, but under biaxial deformations (ϵ), an appreciable difference occurs between P-graphene and N-silicene as we discuss below. In the case of P-graphene we can observe two regimes (see Fig. 1a), for 0 to 5% of strain the BL is almost constant while P is completely out of the plane, followed by a reduction and then a linear increment from 5 to 10%. From 0 to 5% the BA increases with deformation and from 5 to 10% the angle becomes constant $\theta = 120^\circ$ (see Fig. 1c), indicating that the system becomes flat as pristine graphene for deformations larger than 5%. For N-silicene, in Fig. 1b we can see that the BL has a monotonic increase with strain, although around of 9% it seems to reach a maximum. With respect to the BA in N-silicene under strain, interestingly, we can see in Fig. 1d) that biaxial strain does not affect the θ_{SiNSi} , remaining almost constant in the whole range of deformations 0-10%. This means that for the N atom is more favorable to be almost aligned to their first nearest neighbors. This behavior is an effect of the strong hybridization between the N and Si orbitals, avoiding a buckled configuration around N.

3.2. Electronic and magnetic properties

In carbon-based magnetism, it has been proposed that the origin of *sp*-magnetism can be explained by the Stoner theory adapted to the case of a narrow impurity band [24], where a paramagnetic system becomes unstable with respect to the ferromagnetic case when a high density of states exists at the Fermi level. The Stoner criterion for the existence of ferromagnetism is $IN(E_F) > 1$, where I is the Stoner parameter and $N(E_F)$ is the density of states (DOS) of the paramagnetic case at Fermi level. It has been suggested that this criterion is useful to describe the emergence of magnetism in systems with *sp*-electrons, particularly in graphene nanostructures with vacancies or with adsorbed hydrogen atoms [2, 4, 25, 26]. The cases of substituted graphene and even silicene are not the exception. However, for these substitutional cases, the role of the specific impurity is important, otherwise, other *sp*-impurities could induce magnetism in graphene and silicene. An alternative to the Stoner model for the ferromagnetism occurring in a narrow impurity band can be found in Appendix A, which is based on the proposal of Edwards and Katsnelson [24] and the work of Gruber *et al.*[27]

In Fig. 2 the paramagnetic electronic band structure of P-graphene (left) and the N-silicene (right) are shown at the unstrained state for the three different values of concentration ($c = 1.4, 2.0$ and 3.1%). As it is well known, the band structure of graphene and silicene shows a linear dispersion around the Fermi level in the K point, the so-called Dirac cones. From Fig. 2, it is observed that for concentrations of 2.0 and 3.1% this linearity disappears with doping, and in fact we find a band gap opening and a narrow impurity band at the Fermi level (band in red color). For the concentration of 1.4% the band structure shows differences with respect to the other two concentrations due to band folding effect by the use of the supercells [28]. For this concentration, the K point of the unit cell is folded to the Γ point of the supercell as Figs. 2a and 2b show. Besides, the band gap opening does not occur, but the impurity band is present. It is interesting to note that the dispersion of the impurity band is larger in N-silicene with respect to P-graphene. Nevertheless, in both systems the dispersion of the impurity band increases with the concentration. A further characterization of the impurity band was done and we find that for both systems the Fermi level is at half-filling and that the maximum occupancy is 1.0 . Additionally, the value of the impurity bandwidth (W_{imp}) for the concentration of 2.0% in P-graphene and N-silicene is 65 and 84 meV, respectively. This very narrow impurity-band is able to produce a sharp peak in the Density of States (DOS) at Fermi level. Hence, an electronic instability in the paramagnetic state is expected from the high value of $N(E_F)$, in particular a band-splitting induced by spin polarization, generating a net magnetic moment in the system.

In order to have more physical insight on this instability, we have performed first-principles calculations for the total-energy as a function of the magnetic moment in the supercell using the Fixed Spin Moment (FSM) method [29]. In Fig. 3, we show the calculated values (symbols) of the total-energy as a function of the spin magnetic

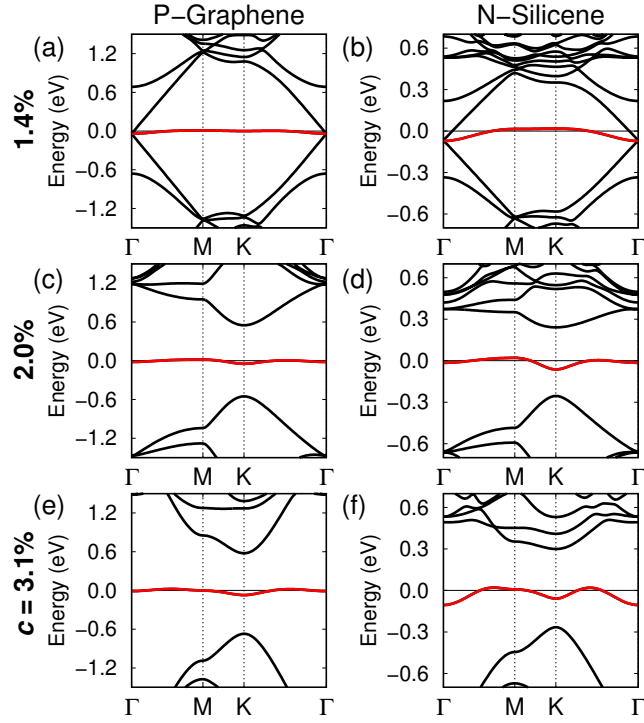


Figure 2. Electronic band structure for P-graphene and N-silicene in the paramagnetic state for the three studied concentrations. The origin of the energy scale has been set at the Fermi level (E_F). The narrow impurity band is emphasized in red.

moment, $E(M)$, for P-graphene and N-silicene for $c = 2.0\%$, using as a reference the total-energy of the paramagnetic case. In both cases the ferromagnetic state has lower energy than the paramagnetic state. The behavior of $E(M)$ indicates that the most stable state is the full polarized state with a spin magnetic moment of $1.0 \mu_B/\text{cell}$, corresponding to strong ferromagnetism [30, 31].

From the model for ferromagnetism in a narrow impurity band described in Appendix A, we have that in the case of half-filling, maximum occupancy $N_0 = 1$, and assuming the rigid band splitting, the total energy as a function of the magnetic moment is thus given by

$$E(M) = E_0 + \frac{M^2}{4} (W_{imp} - U), \quad (2)$$

where E_0 corresponds to the reference energy, for instance the total energy of the paramagnetic state, and U to the Coulomb type interaction. Thus, the condition for spontaneous magnetization is $U/W_{imp} > 1$ [30, 27, 31]. The values for W_{imp} where obtained previously from the paramagnetic band structure, 65 meV for P-graphene and 84 meV for N-silicene at $c = 2.0\%$. Hence, to obtain the values for U , we have fitted (2) to the calculated values of $E(M)$, solid line in Fig. 3, resulting in $U = 250$ meV for P-graphene and $U = 172$ meV for N-silicene. Therefore, U/W_{imp} is 3.8 and 2.0 for P-graphene and N-silicene, respectively, fulfilling the Stoner-type criterion $U/W_{imp} > 1$. From this quantitative analysis of the total-energy as a function of the spin magnetic

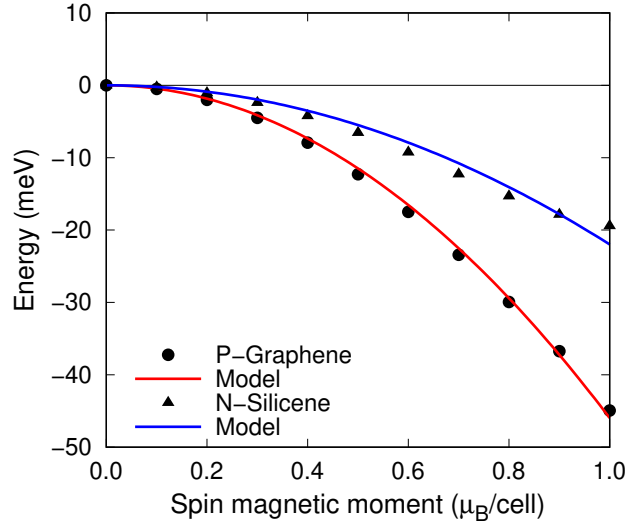


Figure 3. Energy as a function of the magnetic moment for P-graphene and N-silicene at $c = 2\%$, calculated using the fixed-spin moment method (symbols). The solid line corresponds to the fit of $E(M)$ given by eq. (2) to the calculated values (symbols).

moment using a Stoner-type model, it is clear that the value of U in these systems is small. Consequently, the spontaneous polarization in P-graphene and N-silicene is driven by the very small value of W_{imp} .

The electronic band structure and DOS for the spin-polarized state for P-graphene and N-silicene are presented in Figures 4 and 5, respectively. The spin-up states are indicated in red color and the spin-down states in blue color. For reference, also we have included the paramagnetic bands in grey color. The largest spin-splitting is for the impurity band, but the host bands also show an important spin-splitting, indicating that the spin-polarization is not only localized at the impurity atom. It is also interesting to note that the impurity bandwidth for spin-down is larger than for the spin-up, indicating that the spin-polarization of the impurity band is not a rigid-band splitting. The impurity band splitting is a result of the exchange interaction between the electrons in the narrow impurity band. Thus, in order to characterize the exchange interaction, we have calculated the spin-splitting of the impurity band (Δ_s) by taking a weighted average in the first Brillouin zone. The values for Δ_s in P-graphene and N-silicene are 267 meV and 137 meV, respectively.

The analysis of the density of states revealed that the high DOS at Fermi level in Figures 4 and 5, which gives rise to magnetism comes from the hybridization of the orbitals at the impurity atom and the orbitals at the atoms which belong to the sublattice adjacent to the impurity. For P-graphene the localized state at the Fermi level have contributions of s and p_z orbitals from P, and from p_z orbital of C atoms. In the case of N-silicene, the main contributions to the peak at the DOS that causes the instability come from the s and p_z orbitals from N, s and p_z from Si, and a small contribution p_x and p_y , which makes sense due to the buckled structure of silicene.

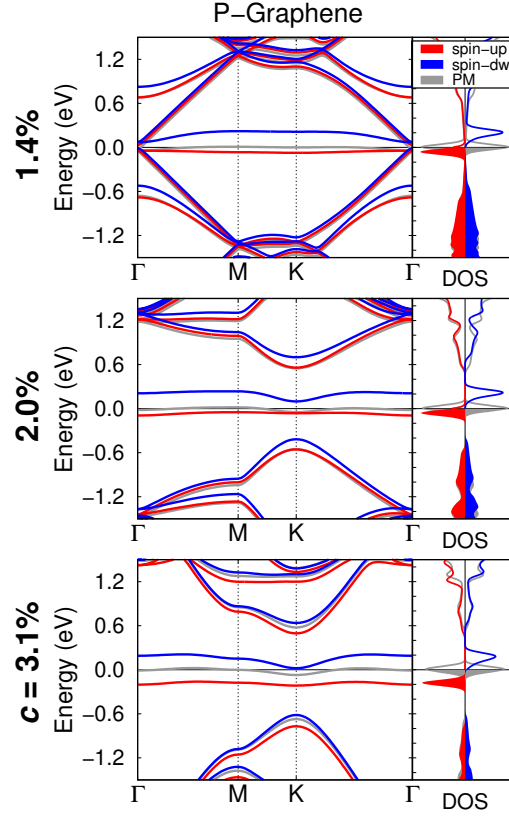


Figure 4. Spin-polarized electronic band structure for P-graphene at the three studied concentrations. The red and blue lines correspond to the spin-up and spin-down, respectively. For reference, the paramagnetic case is included in grey color.

As a first approximation to the analysis of the local magnetic moments distribution, we analyzed the Löwdin charges for each atom. On the top of Fig. 6 we have shown iso-surfaces of the spin electronic density charge ($\rho^\uparrow - \rho^\downarrow$) whereas the local magnetic moment distributions are plotted at the bottom. The red color corresponds to majority spin density and blue (green) color to minority spin density for P-graphene (N-silicene). For the bottom of Fig. 6, the color represents the contribution to the local magnetic moment from σ ($s+p_x+p_y$) orbitals in red and π (p_z) orbitals in blue. The spin density charge plots are presented in an extended supercell which involves a supercell with its first six neighbors. We can observe a spin distribution spread on all of the lattice, where the impurity and their first atomic three neighbors have a majority spin density. Interestingly, each kind of spin density is majority on each sublattice. The dashed black line is used to define a radial distance with respect to the impurity. Inside this circumference, we plot the local magnetic moments as a function of the radial distance and for each distance, we have performed a sum according to the number of the atoms at that distance. It is clear that the local magnetic moment distribution is not homogeneous on the lattice, but the pattern is the same in both P-graphene and N-silicene. Interestingly, only a small fraction of the total magnetic moment is located at the impurity atom.

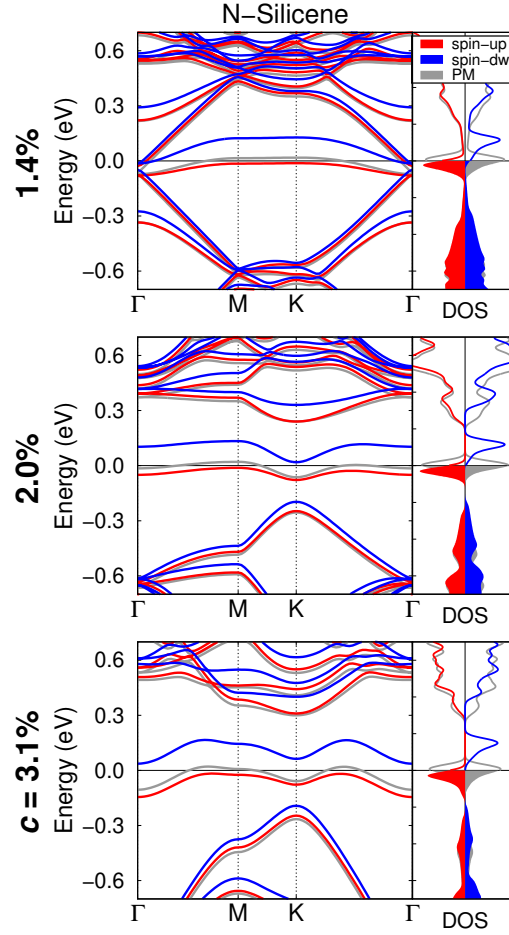


Figure 5. Spin-polarized electronic band structure for N-silicene at the three studied concentrations. The red and blue lines correspond to the spin-up and spin-down, respectively. For reference, the paramagnetic case is included in grey color.

Thus, from the present analysis we can now answer the question; why P-graphene and N-silicene are magnetic? According to our observations, there are two fundamental reasons: *i*) the impurity have an electronic configuration with one more electron than the host material, and *ii*) the impurity induces a very narrow band at Fermi level.

After the analysis and characterization of the electronic structure and the spin-magnetic moment for unstrained P-graphene and N-silicene, in Fig. 7, we show the evolution of the electronic structure with strain for P-graphene and N-silicene at $c = 2.0\%$ in the paramagnetic state. The band structure along the high symmetry paths of the first Brillouin zone in P-graphene shows a narrow band around the Fermi level, except in the K point where a parabolic dispersion is observed. As the strain increases, this effect is more pronounced. The electronic behavior in N-silicene under isotropic deformation shows a different evolution. The nearly flat impurity band around the Fermi level along the high symmetry paths with a small parabolic dispersion around the K point observed for $\varepsilon = 0\%$, is strongly distorted under biaxial strain. As the deformation is increased the flat character disappears and shows parabolic dispersion

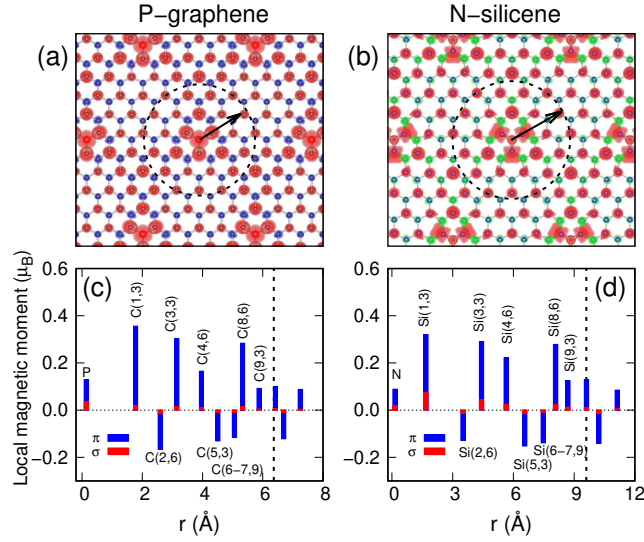


Figure 6. Spin density charge (top) and the π and σ contributions to the local magnetic moments as a function of radial distance from the impurity atom (bottom) for P-graphene and N-silicene at $c = 2\%$. The two indexes at each C or Si atom position represents the order of nearest neighbor with respect to the impurity and the number of nearest neighbors.

around the K and Γ points. Thus, we find that in both systems the dispersion of the impurity band increases with the biaxial strain.

In Fig. 8 we show the behavior of W_{imp} as a function of the biaxial strain for P-graphene and N-silicene for the three studied concentrations, as obtained from the paramagnetic band structure. For P-graphene, we can see that W_{imp} follows a linear behavior with the applied strain in the range 0-5% of deformations for the three concentrations, with a large step at $\varepsilon \sim 5\%$. For N-silicene, the behavior of W_{imp} with the biaxial strain is strongly dependent on the concentration. For instance, for $c = 3.1\%$ the impurity bandwidth increases monotonically with the deformation, while for $c = 1.4\%$ the W_{imp} shows a minimum around 4% of deformation. According to the narrow impurity band model discussed above, these results anticipate the loss of magnetism in both systems, but the behavior of the magnetic moment with the biaxial strain and the concentration dependence for each system will be different.

In Fig. 9, the spin-polarized electronic band structure and DOS for P-graphene and N-silicene at $c = 2.0\%$ under biaxial strain are presented. In both systems we find that the impurity band dispersion increases with the strain for both spin channels, inducing overlapping of the spin-up and spin-down bands, as can be seen in the DOS. At the same time, the spin-splitting of the impurity band decreases. For this concentration, we can see that in both systems the spin-splitting vanishes at $\varepsilon = 6\%$, indicating that the magnetism has been lost.

Interestingly, for P-graphene at $\varepsilon = 6\%$ we recover a linear dispersion around K point as in graphene pristine (Fig. 9d), however, the Fermi level is located above

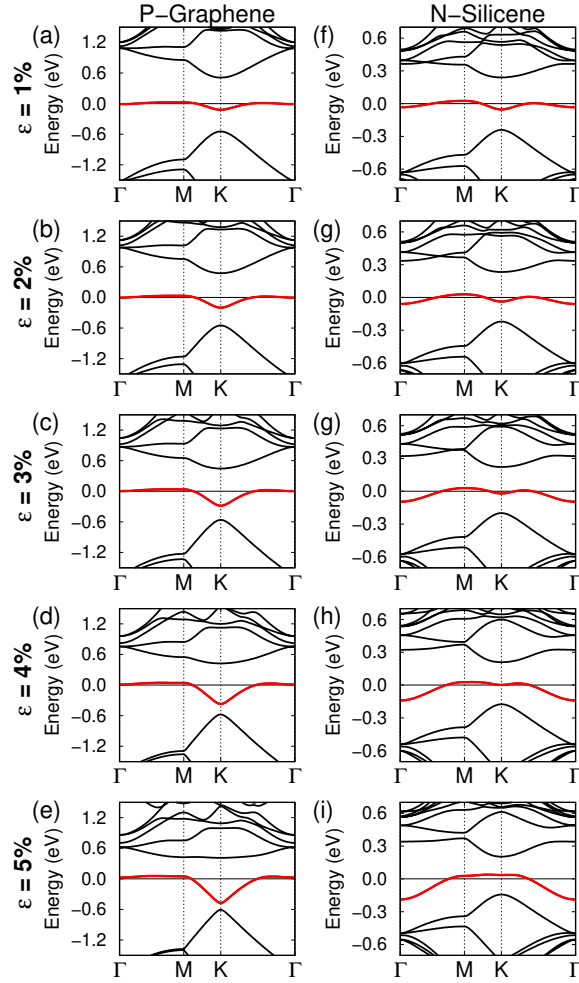


Figure 7. Electronic band structure for P-graphene and N-silicene at $c = 2.0\%$ in the paramagnetic state as a function of the strain. The origin of the energy scale has been set at the Fermi level (E_F). The impurity band is emphasized in red color.

the Dirac point corresponding to electron doped graphene. For this deformation, as mentioned before, the system recovers its flatness, showing the close relation between structural and electronic properties. The electronic structure of N-silicene under isotropic deformation (Fig. 2e-h) shows a different evolution with respect to P-graphene. In this case, the impurity band at $\varepsilon = 0\%$ shows a parabolic dispersion around the K point and a nearly flat character along the high symmetry paths. However, with deformation the evolution of the impurity band leads to a parabolic nature around K and Γ points, with hole character at K and electron character at Γ . We notice that for N-silicene under strain, in contrast to P-graphene, we do not recover the Dirac cones (see Fig. 9h). Thus, the electronic character of N-silicene under biaxial strain in the non-magnetic state will be of a normal metal.

The evolution of the magnetic moment as a function of the strain for each concentration is shown in Fig. 10. For the unstrained case both systems are magnetic

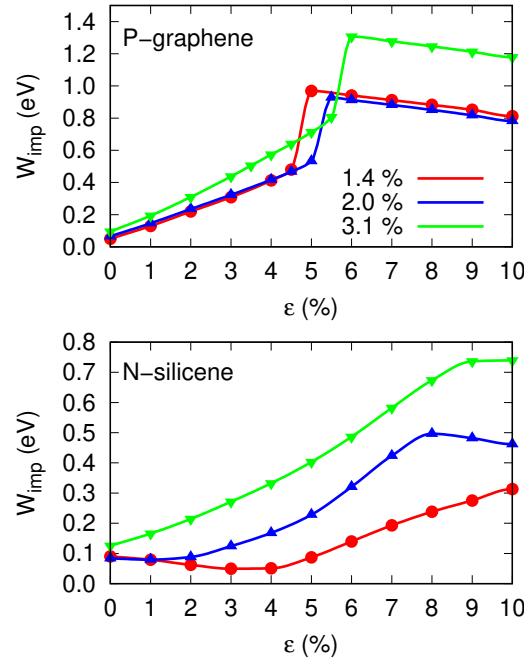


Figure 8. Evolution of the impurity bandwidth (W_{imp}) as a function of the strain (ε) for P-graphene and N-silicene at the three studied concentrations (1.4, 2.0, and 3.1%) in the paramagnetic state.

with a net magnetic moment of $1.0 \mu_B/\text{cell}$ regardless of concentration. Under strain, the magnetic moment changes from 1.0 to $0 \mu_B/\text{cell}$, indicating that a magnetic transition appears when a biaxial strain is applied. Although P-graphene presents almost similar transition with the doped concentration, N-silicene has a strong dependence on the doping concentration. Nevertheless, a common feature is that in both systems we have a range of deformations starting from $\varepsilon = 0\%$ where the magnetic moment remain constant ($M = 1.0$), a second range where the magnetic moment begins to decrease with strain ($0 < M < 1.0$) and a third range where the system is non-magnetic ($M = 0$), after reaching the critical deformation where $M \rightarrow 0$.

In order to understand the behavior of the magnetic moment in P-graphene and N-silicene with the applied strain, we return to the model of ferromagnetism in a narrow impurity band, described in detail in the Appendix A. To simplify the analysis we will assume that the value of U does not change with strain. This consideration comes from a further analysis of the spin-splitting for the impurity band and the magnetic moment as a function of the strain, which shows a practically constant behaviour of U at different deformations. In this case both systems are at half-filling and the maximum occupancy is $N_0 = 1$, therefore the full polarized state remains as long as $W_{\text{imp}} < U$. This condition is fulfilled in the first range where the spin magnetic moment is $1.0 \mu_B/\text{cell}$ with the system in the strong ferromagnetic state. In Fig. 8, we can see that for P-graphene the impurity bandwidth W_{imp} increases linearly with strain independently of the doping concentration, with practically the same slope up to $\varepsilon \sim 5\%$. This is the transition region

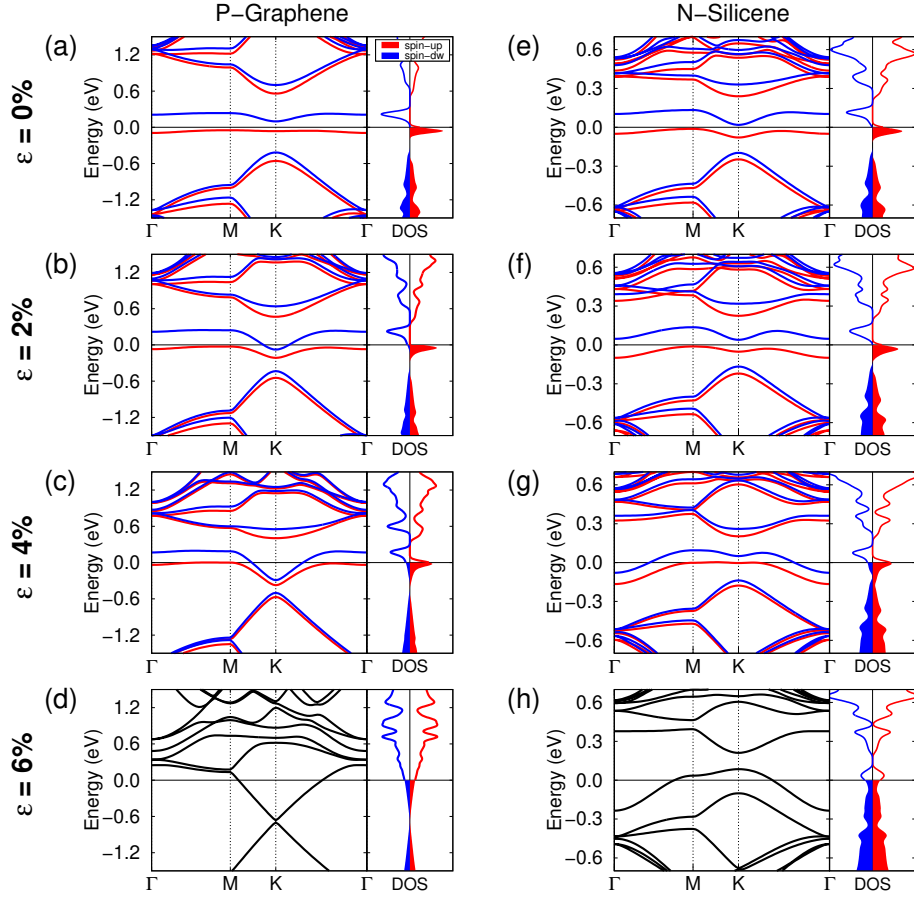


Figure 9. Spin-polarized electronic band structure for P-graphene and N-silicene at $c = 2.0\%$ as a function of the strain. The origin of the energy scale has been set at the Fermi level (E_F).

where the system is in the weak ferromagnetic state, characterized by an unsaturated spin-up band and a magnetic moment $M < 1.0\mu_B/\text{cell}$. In the case of N-silicene, the picture is the same, however the details of the transition are strongly dependent on the doping concentration as a result of the different behavior of W_{imp} with strain (see Fig.8). For the analysis of N-silicene, we will start with the highest concentration $c = 3.1\%$, where the W_{imp} increases almost linearly with the biaxial strain. Thus, in this particular case the transition of the magnetic moment is similar to P-graphene. For N-silicene at $c = 2.0\%$ the value of W_{imp} remain almost constant up to $\varepsilon \sim 3\%$, extending the first region corresponding to the strong ferromagnetic state, but with a narrower transition region. Finally, for N-silicene at $c = 1.4\%$ we can see in Fig. 8 that W_{imp} decreases in the range of 0-4% for the strain, reaching a minimum value at $\varepsilon = 4\%$, and then increase linearly with a very small slope. In this way, the strong ferromagnetic state in N-silicene at $c = 1.4\%$ extends up to $\varepsilon = 4\%$ and the wide transition region up to $\varepsilon = 8.5\%$.

To conclude, despite the differences in the behavior of the magnetic moment with the biaxial strain for P-graphene and N-silicene, in particular the strong dependence in

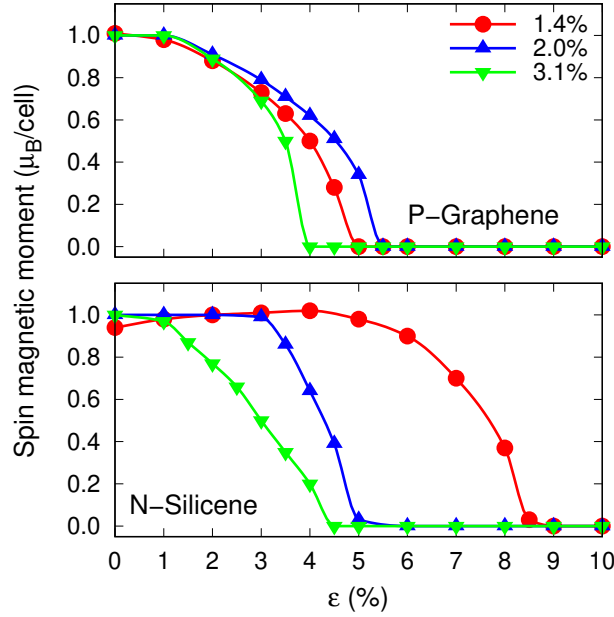


Figure 10. Spin magnetic moment as a function of biaxial strain for P-graphene and N-silicene at the three studied concentrations (1.4, 2.0, and 3.1%).

the case of N-silicene with the doping concentration, a common feature was recognized and characterized, emerging the picture depicted in Fig. 11. So, we have that for low strain values the system remains in the strong ferromagnetic (SF) state, followed by a transition region corresponding to a weak ferromagnetic (WF) state with a impurity band partially polarized, and finally the non-magnetic region after reaching the critical strain where the ground state corresponds to a paramagnetic (PM) state. This picture, was confirmed performing fixed spin moment calculations of the total energy as a function of the spin magnetic moment, for three values of biaxial deformations 0, 4.0 and 7.0% corresponding to SF, WF, and PM states, respectively. The results are presented in the inset of Fig. 11. The calculated plots for $E(M)$ are in close agreement with the general model of itinerant electrons in a narrow band [31] .

4. Conclusions

For P-graphene and N-silicene the origin of the magnetism is result of a partially filled very narrow band at Fermi level induced by the impurity. This narrow impurity band causes an electronic instability which favours a magnetic state, which is characterized by magnetic moment of $1.0 \mu_B/\text{cell}$ corresponding to a full-polarized impurity band. We found that a Stoner-type model describing the electronic instability of the narrow impurity band accounts for the origin of *sp*-magnetism in P-graphene and N-silicene. The evolution of the spin magnetic moment as a function of the biaxial strain is mainly governed by the behavior of the impurity bandwidth with the applied strain. Thus, the biaxial strain evolves the systems from a strong ferromagnetic state to a paramagnetic

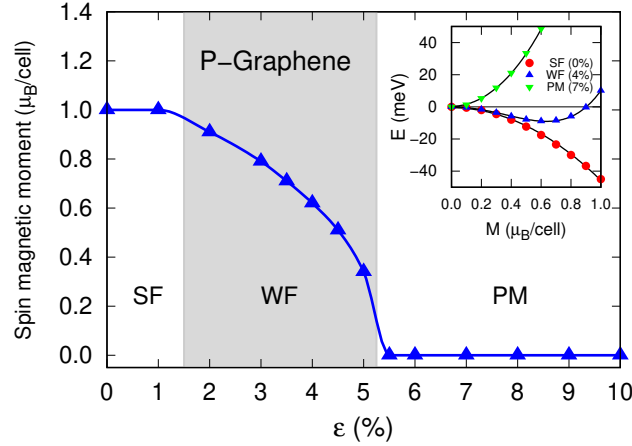


Figure 11. Evolution of the spin-magnetic moment as a function of the strain for P-graphene at $c = 2\%$ indicating the regions for strong-ferromagnetism (SF), weak-ferromagnetism (WF) and paramagnetic (PM) behaviors. In the inset the calculated $E(M)$ using the fixed-spin moment method (symbols), for deformations of 0.0, 4.0, and 7.0%, corresponding to SF, WF, and PM states, respectively.

state, with a transition region corresponding to a weak ferromagnetic state characterized by a partially polarized impurity band. Furthermore, it has been demonstrated that with strain it is possible to modulate the spin magnetic moment and induce a magnetic quantum phase transition. Consequently, the control and manipulation of the magnetic properties in these two-dimensional magnetic systems are technologically attractive for the potential applications in spintronics and spin-based quantum computation systems, using strain engineering as an effective way to modulate the magnetic properties in 2D-materials.

5. Acknowledgments

The authors thankfully acknowledge the computer resources, technical expertise and support provided by the Laboratorio Nacional de Supercómputo del Sureste de México. J.H.T. acknowledges a student fellowship from the Consejo Nacional de Ciencia y Tecnología (Conacyt, México) and VIEP-BUAP. M.E.C.Q. gratefully acknowledges a posdoctoral fellowship from Conacyt-México. This research was supported by Conacyt-México under grant No. 288344.

Appendix A. Model of narrow impurity band ferromagnetism

According to the paramagnetic band structures at zero deformation, a narrow impurity band at Fermi level is present in P-graphene and N-silicene. Thus, the origin of magnetism could be attributed to this band because the exchange interaction induces a spin-splitting. Edwards and Katsnelson [24] restated the conventional Stoner criteria

$IN(E_F) > 1$ to the case of a narrow impurity band where the density of states at Fermi level is approximated by $N(E_F) = n_{imp}/W_{imp}$, being n_{imp} the impurity density and W_{imp} the width of the impurity rectangular band. On the other hand, Gruber et al. [27] using a mean-field version of the Hubbard like interaction describe the band energy of the electronic states for the impurity band for each spin channel, as follows:

$$E = E_{band}^{\uparrow} + E_{band}^{\downarrow} + Un^{\uparrow}n^{\downarrow}, \quad (\text{A.1})$$

where the terms E_{band} within the tight-binding approximation are

$$E_{band}^{\uparrow} = \int_{E_{min}^{\uparrow}}^{E_F} (E - E_c^{\uparrow})N^{\uparrow}(E)dE, \quad (\text{A.2})$$

$$E_{band}^{\downarrow} = \int_{E_{min}^{\downarrow}}^{E_F} (E - E_c^{\downarrow})N^{\downarrow}(E)dE, \quad (\text{A.3})$$

here E_c^{\uparrow} and E_c^{\downarrow} are the center of the band for each spin channel which suffers an energy shift in the spin-polarized case with respect to the paramagnetic case, in order to have a non-zero magnetic moment. The E_F , E_{min}^{\uparrow} and E_{min}^{\downarrow} are the Fermi level and the lower limits of each band. The third term in (A.1), corresponds to a Coulomb type interaction U suppressing double occupancy and n^{\uparrow} (n^{\downarrow}) is the number of the spin-up (spin-down) electrons in the band. The number of electrons in each spin band can be obtained from

$$n^{\uparrow} = \int_{E_{min}^{\uparrow}}^{E_F} N^{\uparrow}(E)dE, \quad (\text{A.4})$$

$$n^{\downarrow} = \int_{E_{min}^{\downarrow}}^{E_F} N^{\downarrow}(E)dE. \quad (\text{A.5})$$

The total number of electrons Z is given by

$$Z = n^{\uparrow} + n^{\downarrow}, \quad (\text{A.6})$$

and the magnetic moment M

$$M = n^{\uparrow} - n^{\downarrow}. \quad (\text{A.7})$$

Now, according to the Friedel's model [30], we assume a DOS with rectangular shape for each spin channel. In Fig. A1 we show the paramagnetic and spin-polarized case according to this model. Thus, the density of states $N(E)$ for each spin channel is constant and is given by

$$N^{\uparrow}(E) = \frac{N_0}{W^{\uparrow}}, \quad (\text{A.8})$$

$$N^{\downarrow}(E) = \frac{N_0}{W^{\downarrow}}, \quad (\text{A.9})$$

where N_0 is maximum occupancy of the band and W^{\uparrow} (W^{\downarrow}) is the bandwidth for each spin-up (spin-down).

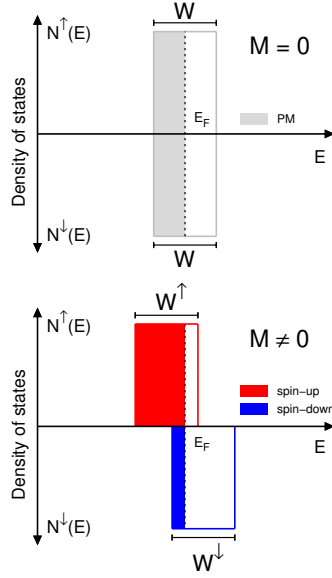


Figure A1. Density of states of the impurity band for the paramagnetic (top) and spin polarized (bottom) states in the rectangular model.

With (A.2) and (A.8) we rewrite the band energy for the spin-up band

$$E_{band}^{\uparrow} = \int_{E_{min}^{\uparrow}}^{E_F} (E - E_c^{\uparrow}) \frac{N_0}{W^{\uparrow}} dE, \quad (\text{A.10})$$

$$E_{band}^{\uparrow} = \frac{N_0}{W^{\uparrow}} \left[\frac{(E - E_c^{\uparrow})^2}{2} \right]_{E_{min}^{\uparrow}}^{E_F}. \quad (\text{A.11})$$

The lower limit corresponds to $E_{min}^{\uparrow} = E_c^{\uparrow} - (W^{\uparrow}/2)$ and the Fermi energy is obtained from (A.4) using (A.8)

$$n^{\uparrow} = \left[\frac{N_0}{W^{\uparrow}} E \right]_{E_{min}^{\uparrow}}^{E_F} = \frac{N_0}{W^{\uparrow}} \left[E_F - \left(E_c^{\uparrow} - \frac{W^{\uparrow}}{2} \right) \right], \quad (\text{A.12})$$

$$E_F = \frac{n^{\uparrow} W^{\uparrow}}{N_0} + E_c^{\uparrow} - \frac{W^{\uparrow}}{2}. \quad (\text{A.13})$$

With $E_{min}^{\uparrow} = E_c^{\uparrow} - (W^{\uparrow}/2)$ and E_F given by (A.13), we evaluate E_{band} in (A.11)

$$E_{band}^{\uparrow} = \frac{N_0}{2W^{\uparrow}} \left[\left(\frac{n^{\uparrow} W^{\uparrow}}{N_0} + E_c^{\uparrow} - \frac{W^{\uparrow}}{2} - E_c^{\uparrow} \right)^2 - \left(E_c^{\uparrow} - \frac{W^{\uparrow}}{2} - E_c^{\uparrow} \right)^2 \right] \quad (\text{A.14})$$

and simplifying, we arrive to:

$$E_{band}^{\uparrow} = \frac{W^{\uparrow}}{2} \left[\frac{n^{\uparrow 2}}{N_0} - n^{\uparrow} \right]. \quad (\text{A.15})$$

In the same way, it is found that E_{band}^{\downarrow} is:

$$E_{band}^{\downarrow} = \frac{W^{\downarrow}}{2} \left[\frac{n^{\downarrow 2}}{N_0} - n^{\downarrow} \right]. \quad (\text{A.16})$$

Replacing the expressions given in (A.15), (A.16) of E_{band}^\uparrow and E_{band}^\downarrow in (A.1), we obtain that

$$E = \frac{W^\uparrow}{2} \left(\frac{n^{\uparrow 2}}{N_0} - n^\uparrow \right) + \frac{W^\downarrow}{2} \left(\frac{n^{\downarrow 2}}{N_0} - n^\downarrow \right) + U n^\uparrow n^\downarrow. \quad (\text{A.17})$$

Now, from (A.6) and (A.7), n^\uparrow and n^\downarrow can be expressed in terms of the magnetic moment M and the total number of electrons Z

$$n^\uparrow = \frac{Z + M}{2}, \quad (\text{A.18})$$

$$n^\downarrow = \frac{Z - M}{2}. \quad (\text{A.19})$$

Using this expressions for n^\uparrow and n^\downarrow in (A.17), we obtain an expression for the energy E as a function of M

$$\begin{aligned} E(M) = & \frac{Z^2}{4} \left(\frac{W^\uparrow + W^\downarrow}{2N_0} + U \right) - \frac{Z}{4} (W^\uparrow + W^\downarrow) \\ & + \frac{M}{4} (W^\uparrow - W^\downarrow) \left(\frac{Z}{N_0} - 1 \right) \\ & + \frac{M^2}{4} \left(\frac{W^\uparrow + W^\downarrow}{2N_0} - U \right). \end{aligned} \quad (\text{A.20})$$

The first two terms are independent of M , the third term is a linear dependence of M , however in the case of half-filling ($N_0 = Z$) this term vanishes. The last term has a quadratic dependence of M and for spontaneous magnetization needs to be less than 0:

$$\frac{W^\uparrow + W^\downarrow}{2N_0} - U < 0, \quad (\text{A.21})$$

which can be written as

$$\frac{2N_0 U}{W^\uparrow + W^\downarrow} > 1. \quad (\text{A.22})$$

For the case of a rigid band splitting ($W^\uparrow = W^\downarrow$), the condition for spontaneous magnetization is:

$$U \frac{N_0}{W} > 1. \quad (\text{A.23})$$

We can see that this condition is a Stoner-like criterion, since the ratio N_0/W is the density of states per spin channel in the present model. Thus, it is clear that for a narrow impurity band where W is very small, this condition can be fulfilled even for small or moderate U values and low occupancy. The present model should be suitable for systems that present a full-polarized impurity band, i.e. in the strong ferromagnetism regime.

References

- [1] K.S. Novoselov, A.K. Geim, S.V. Morozov, D. Jiang, Y. Zhang, S.V. Dubonos, et al., Electric field effect in atomically thin carbon films, *Science* **306** (2004) 666-669.
- [2] O.V. Yazyev and L. Helm, Defect-induced magnetism in graphene, *Phys. Rev. B* **75** (2007) 125408.
- [3] R.R. Nair, I.L. Tsai, M. Sepioni, O. Lehtinen, J. Keinone, A.V. Krasheninnikov, et al., Dual origin of defect magnetism in graphene and its reversible switching by molecular doping, *Nat. Commun.* **4** (2013) 2010.
- [4] H. González-Herrero, J.M. Gómez-Rodríguez, P. Mallet, M. Moaied, J.J. Palacios, C. Salgado, et al., Atomic-scale control of graphene magnetism by using hydrogen atoms, *Science* **352** (2016) 437-441.
- [5] E.J.G. Santos, A. Ayuela, and D. Sánchez-Portal, First-principles study of substitutional metal impurities in graphene: structural, electronic and magnetic properties, *New J. Phys.* **12** (2010) 053012.
- [6] D. Pesin and A.H. MacDonald, Spintronics and pseudospintronics in graphene and topological insulators, *Nat. Mater.* **11** (2012) 409.
- [7] W. Han, R.K. Kawakami, M. Gmitra, and J. Fabian, Graphene spintronics, *Nat. Nanotechnol.* **9** (2014) 794.
- [8] N. Rohling and G. Burkard, Universal quantum computing with spin and valley states, *New J. Phys.* **14** (2012) 083008.
- [9] G. Coudourier-Maruri, Y. Omar, R. de Coss, and S. Bose, Graphene-enabled low-control quantum gates between static and mobile spins, *Phys. Rev. B* **89** (2014) 075426.
- [10] J. Dai and J. Yuan, Adsorption of molecular oxygen on doped graphene: Atomic, electronic, and magnetic properties, *Phys. Rev. B* **81** (2010) 165414.
- [11] J. Dai and J. Yuan, Modulating the electronic and magnetic structures of P-doped graphene by molecule doping, *J. Phys.: Condens. Matter* **22** (2010) 225501.
- [12] H.M. Wang, H.X. Wang, Y. Chen, Y.J. Liu, J.X. Zhao, Q.H. Cai, et al., Phosphorus-doped graphene and (8, 0) carbon nanotube: structural, electronic, magnetic properties, and chemical reactivity, *Appl. Surf. Sci.* **273** (2013) 302-309.
- [13] P.A. Denis, Band gap opening of monolayer and bilayer graphene doped with aluminium, silicon, phosphorus, and sulfur, *Chem. Phys. Lett.* **492** (2010) 251-257.
- [14] J. Sivek, H. Sahin, B. Partoens, and F.M. Peeters, Adsorption and absorption of boron, nitrogen, aluminum, and phosphorus on silicene: Stability and electronic and phonon properties, *Phys. Rev. B* **87** (2013) 085444.
- [15] S. Li, Z. Ao, J. Zhu, J. Ren, J. Yi, G. Wang, et al., Strain controlled ferromagnetic-antiferromagnetic transformation in Mn-doped silicene for information transformation devices, *J. Phys. Chem. Lett.* **8** (2017) 1484-1488.
- [16] R. Zheng, Y. Chen, and J. Ni, Highly tunable magnetism in silicene doped with Cr and Fe atoms under isotropic and uniaxial tensile strain, *Appl. Phys. Lett.* **107** (2015) 263104.
- [17] E.J.G. Santos, A. Ayuela, and D. Sánchez-Portal, Strain-tunable spin moment in Ni-doped graphene *J. Phys. Chem. C* **116** (2012) 1174-1178.
- [18] P. Giannozzi, S. Baroni, N. Bonini, M. Calandra, R. Car, C. Cavazzoni, et al., QUANTUM ESPRESSO: a modular and open-source software project for quantum simulations of materials, *J. Phys.: Condens. Matter* **21** (2009) 395502.
- [19] A.D. Corso, Pseudopotentials periodic table: From H to Pu, *Comput. Mater. Sci* **95** (2014) 337-350.
- [20] J.P. Perdew, K. Burke, and M. Ernzerhof, Generalized Gradient Approximation Made Simple, *Phys. Rev. Lett.* **77** (1996) 3865.
- [21] H.J. Monkhorst and J.D. Pack, Special points for Brillouin-zone integrations, *Phys. Rev. B* **13** (1976) 5188.
- [22] M. Methfessel and A.T. Paxton, High-precision sampling for Brillouin-zone integration in metals,

- Phys. Rev. B **40** (1989) 3616.
- [23] I. A. Pašti, A. Jovanovi, A. S. Dobrota, S. V. Mentus, B. Johansson and N. V. Skorodumova, Atomic adsorption on graphene with a single vacancy: systematic DFT study through the periodic table of elements, Phys. Chem. Chem. Phys. **20**, (2018) 858-865 .
 - [24] D.M. Edwards and M.I. Katsnelson, High-temperature ferromagnetism of sp electrons in narrow impurity bands: application to CaB_6 , J. Phys.: Condens. Matter **18** (2006) 7209.
 - [25] O.V. Yazyev, Emergence of magnetism in graphene materials and nanostructures, Rep. Prog. Phys. **73** (2010) 056501.
 - [26] K.W. Lee and C.E. Lee, Intrinsic Impurity-Band Stoner Ferromagnetism in C_{60}H_n , Phys. Rev. Lett. **106** (2011) 166402.
 - [27] C. Gruber, P.O. Bedolla, and P. Mohn, Covalent magnetism and magnetic impurities, J. Phys.: Condens. Matter **25** (2013) 186002.
 - [28] Y.C. Zhou, H. L. Zhang and W. Q. Deng, A 3N rule for the electronic properties of doped graphene, Nanotechnology **24**, (2013) 225705 .
 - [29] K. Schwarz and P. Mohn, Itinerant metamagnetism in YCo_2 , J. Phys. F: Met. Phys. **14** (1984) 129 .
 - [30] J. Friedel and C.M. Sayers, On the role of d-d electron correlations in the cohesion and ferromagnetism of transition metals, J. Phys. France **38** (1977) 697-705.
 - [31] P. Mohn, *Magnetism in the Solid State, Springer Series in Solid State Sciences, vol. 134*, (Springer, Berlin, 2003), p. 75-79.